BULLETIN OF THE POLISH ACADEMY OF SCIENCES
TECHNICAL SCIENCES
Vol. 52, No. 3, 2004

Performance characteristics of the 1.3-μm oxide-confined edge-emitting quantum-dot (InGa)As/GaAs diode lasers

R. P. SARZAŁA[1]*, M. WASIAK[1], T. CZYSZANOWSKI[1] and W. NAKWASKI[1,2]

[1] Laboratory of Computer Physics, Institute of Physics, Technical University of Łódź, 219 Wólczańska St., 93–005 Łódź, Poland
[2] Center for High Technology Materials, University of New Mexico Albuquerque, NM 87106, 1313 Goddard SE, USA

Abstract. The self-consistent optical-electrical-thermal-gain model of the oxide-confined edge-emitting diode laser has been used to simulate the room-temperature operation of the long-wavelength 1.3-μm quantum-dot (InGa)As/GaAs diode laser. The validity of the model has been verified using some experimental results for comparison. An impact of quantum-dot density on laser operation characteristics as well as on temperature dependence of lasing threshold have been discussed.

Keywords: QD laser, 1.3-μm optical fibre communication, simulation of performance characteristics, quantum dots.

1. Introduction

There are a number of possible solutions to obtain efficient, reliable and high-performance semiconductor lasers for long-wavelength 1.3-μm optical-fibre-window communication systems and 1.3-μm optical switching devices. From among them, the GaInNAs lasers, the GaAsSb lasers, the InAlGaAs lasers and the (InGa)(AsP)/InP lasers fused with (AlGa)As/GaAs mirrors have been believed to be the most advanced ones. Unfortunately, these structures are expensive and their parameters not satisfactory. Recently, however, oxide-confined (InGa)As/GaAs quantum-dot (QD) GaAs-based lasers have been found to exhibit the best performance in this wavelength range. Their technology is relatively simple, based on the natural process of formation of self-organized QDs in the strained epitaxial layer, when its thickness exceeds a critical value (usually a few monolayers). Three-dimensional islands are then spontaneously formed. The next epitaxial layer is used to cover the islands and to finally form the QDs embedded in higher band-gap material matrix [1]. The important advantage of QD lasers is the fact that their fabrication makes use of well established gallium-arsenide lasers technology.

Despite recent impressive achievements of researchers being engaged in manufacturing the 1.3-μm (InGa)As/GaAs GaAs-based QD diode lasers, there is still some room for the technology and structure improvements at their relatively immature development stage. The physics of QD lasers is often essentially different from the physics of conventional diode lasers. Therefore structures regarded as optimal for hitherto existing diode lasers do not have to remain optimal for the QD lasers. Hence present technology of these devices needs some theoretical support to optimise known conventional diode-laser structures or even to discover completely new laser structures specially designed for this purpose. In this paper, the self-consistent optical-electrical-thermal-gain model for the 1.3-μm QD diode laser is developed and its results are presented using the advanced oxide-confined laser structure reported by Park et al. [2] as an example. Comparison between the performance characteristics of this reference laser and the ones determined theoretically is used to examine the model validity and accuracy. An impact of quantum-dot density on laser operation characteristics is discussed. Temperature dependence of lasing threshold is analysed.

2. The model

The computer model used to simulate room-temperature (RT) operation of the laser under consideration consists of four principal parts:

— the optical model describing for successive modes an optical field within the laser resonator,

— the electrical model characterizing both the current spreading (including carrier diffusion) between the top and bottom contacts and the injection of carriers of both kinds into the active region,

— the thermal model characterising generation of a heat flux (nonradiative recombination, reabsorption of spontaneous radiation as well as volume and barrier Joule heating) and its spreading from heat sources towards heat sinks,

— the gain model describing the optical gain process within the quantum-dot active region.

2.1. Optical model. Optical behaviour of the device is modelled using the effective-index method [3]. In this approach, the optically nonuniform multi-layer laser structure is replaced by an equivalent slab waveguide whose refractive-index profile is determined taking into account the geometry and the layer structure of the laser. The structure is divided into sectors of uniform refractive indices within each structure layer, which, however, are usually different in different layers and different in different layer sectors. The co-ordinate system is such that x direction is perpendicular to the layers, whereas z direction is the light propagation one. The optical field $\Phi(x, y)$

* e-mail: rpsarzal@p.lodz.pl

is expressed as:

$$\Phi(x,y) = \Phi_y(y)\,\Phi_{xy}(x,y)\,. \tag{1}$$

Then the two-dimensional optical problem is reduced to two nearly one-dimensional problems described by the equations:

$$\frac{\partial^2\Phi}{\partial x^2} + \frac{\partial^2\Phi}{\partial y^2} + \left[n_R^2(x,y)\,k^2 - \beta^2\right]\Phi = 0 \tag{2}$$

$$\frac{\partial^2\Phi_y}{\partial y^2} + \left[n_{eff}^2(y)\,k^2 - \beta^2\right]\Phi_y = 0 \tag{3}$$

which are solved using standard methods. In the above equations, n_R and n_{eff} are the index of refraction and the effective index of refraction respectively, k is the wave vector and β stands for the propagation constant. The lasing threshold is found from the condition of real propagation constant, which means that for the mode under consideration an imaginary part of its propagation constant vanishes at threshold.

2.2. Electrical model. The electrical model of the laser is based on the Laplace equation:

$$\mathrm{div}\left[\sigma(x,y)\,\mathrm{grad}\,(V(x,y))\right] = 0 \tag{4}$$

where $\sigma(x,y)$ stands for the position-dependent electrical conductivity and $V(x,y)$ is the potential distribution. For all layers of the laser structure with the exception of the active region, the above conductivity σ depends on material composition and its doping, as well as on a local temperature and a local carrier concentration. Generation and recombination phenomena within the active region are usually a source of the non-zero right-hand side of Eq. (4) (known as the Poisson equation in this case). They are, however, taken symbolically into account in the model with the aid of the effective conductivity σ_{pn} of the active region material. Its value is determined using the classical diode equation:

$$\sigma_{pn}(x) = \frac{\beta_{pn} j_{pn}(x)\,d_A}{\ln\left[\frac{j_{pn}(x)}{j_s} + 1\right]} \tag{5}$$

where j_{pn} is the p-n junction current density. Derivation of the diode equation includes all the above mentioned phenomena in a natural way: its empirical parameters β_{pn} and j_s are dependent on the rates of carrier generation and recombination within the active region. Values of both the diode parameter ($\beta_{pn} = 1.5\ \mathrm{V}^{-1}$) and the saturation current density ($j_s = 150\ \mathrm{A/m^2}$) has been determined from experimental plots given in [2, 4]. $d_A = 60$ Å stands for the cumulative thickness of the active layer. The device is assumed to be biased by the U $\approx$ 5 V voltage [4].

To obtain potential profile for the whole laser structure, it should be matched (using the self-consistent approach) with the aid of boundary conditions at all boundaries between the layers. Then the current density distribution $j(x,y)$ may be found from the Ohm law:

$$j(x,y) = -\sigma(x,y)\,\mathrm{grad}\left[V(x,y)\right]. \tag{6}$$

Afterwards carrier density profile $n_A(x)$ within the active layer may be determined from the below-threshold diffusion equation:

$$D_A\frac{d^2 n_A(x)}{dx^2} - B n_A^2(x) - \frac{n_A(x)}{\tau_{nr}} + \frac{j_{pn}(x)}{e d_A} = 0 \tag{7}$$

where $D_A = 5\ \mathrm{cm^2/s}$ [5, 6] is the diffusion coefficient, $B = 9.7\cdot 10^{-17}\ \mathrm{m^3/s}$ [6, 7] stands for the bimolecular recombination constant and $\tau_{nr} = 1.3$ ns [8] is the nonradiative-recombination lifetime.

2.3. The thermal model. In the thermal model of the laser, the heat-conduction equation

$$\mathrm{div}\left[\lambda(x,y)\,\mathrm{grad}\,(T(x,y))\right] = -g_T(x,y) \tag{8}$$

is solved for the whole structure. In the above equation, λ (in W/mK) stands for the position-dependent thermal conduction coefficient and g_T is the analogous volume density of heat sources (in $\mathrm{Wm^{-3}}$). Thermal conductivity of the oxidized $\mathrm{Al}_x\mathrm{O}_y$ layer is assumed equal to that of the sapphire ($\mathrm{Al_2O_3}$). Nonradiative recombination and reabsorption of spontaneous radiation is found to be a main heat source located within the active region of the laser. Additionally, the volume Joule heating in all structure layers and the barrier Joule heating in the contacts are taken into account. Copper heat sink of walls kept at the ambient temperature and of semi-infinite dimensions is assumed because its real sizes are two orders of magnitude larger than those of the laser itself. It has been found in this analysis that, although generally for the laser continuous-wave (CW) RT operation considered here thermal problems should not be neglected, their influence on laser operation is here nearly insignificant because of considerable reduced threshold currents, which is followed by a very little heat generation.

2.4. The gain model. The gain is postulated to be an effect of electrons and heavy holes recombination. The model is based on the assumption that energetic states associated with a quantum dot may be approximated by

— the two-dimensional harmonic oscillator [9, 10], i.e. the two-dimensional parabolic potential, in the (y,z) $p-n$ junction plane and

— the finite (InGa)As/GaAs quantum well of the width equal to the dot height in the x direction.

The first assumption follows from the experimental observation that successive level pairs (in the conduction and the valence bands) are approximately energetically located at equal distances. It is also assumed in the gain calculations that all carriers injected into the active layer are in fact injected into its quantum dots (Bimberg et al. [1], p. 185) Validity of this assumption has been recently confirmed by [11] who have found experimentally the carrier leakage in a similar laser practically insignificant even at high temperatures.

Let $E_{0,e}$ and $E_{0,h}$ denote first electron and hole energy levels in respective bands. Hence successive energy levels

(for $i > 0$) are given by:

$$E_{i,e} = E_{0,e} + i\hbar\omega_e \tag{9}$$

$$E_{i,h} = E_{0,h} + i\hbar\omega_h \tag{10}$$

Supposing that potentials in the conduction and the valence bands are identical, the following equality holds:

$$\frac{\omega_e}{\omega_h} = \sqrt{\frac{m_h}{m_e}} \tag{11}$$

where m_e and m_h are effective masses of electrons in the conduction band and heavy holes in the valence band, respectively.

In unbiased QD lasers, carrier distributions on successive QD energy levels are properly described by the Fermi-Dirac statistics. This statistics remains also valid for relatively long radiative recombination times (Bimberg et al. [1], p. 156). In strongly biased QD lasers, however, some saturation effects in population distributions of carriers on QD levels are observed as a result of slow relaxation processes. Those effects have been found to be proportional to the laser excitation level, i.e. to its output power [12, 13]. Nevertheless, for the threshold laser operation considered here, non-equilibrium distribution of carriers in QDs may be neglected [12].

Quasi-Fermi levels F_e and F_h of the above carriers are determined by the following equations

$$\frac{n_A}{N_D} = \sum_{i=1}^{\infty} \frac{2\,i}{1 + \exp\left(\frac{E_{i,e} - F_e}{k_B T}\right)} \tag{12}$$

$$\frac{n_A}{N_D} = \sum_{i=1}^{\infty} \frac{2\,i}{1 + \exp\left(\frac{E_{i,h} - F_h}{k_B T}\right)} \tag{13}$$

where i in a nominator is associated with a level degeneration, k_B is the Boltzmann constant, n_A is the active-region electron (hole) concentration and N_D is the volume density of dots related to the analogous surface density N in the following way.

$$N_D = \frac{N}{h_x} \tag{14}$$

with h_x — the dot height.

Since broadening related to various dot sizes is much stronger than analogous broadening associated with finite carrier lifetime, we can neglect the latter. Thus we avoid integration in the gain formula:

$$g(E) = \frac{\pi\hbar e^2}{c n_R m_0^2 \varepsilon_0} \frac{N_D}{E} |M|^2 \rho_{QD}(E) \left[f_e(E_e) - f_h(E_h)\right] \tag{15}$$

where c stands for the light velocity in vacuum, n_R is the index of refraction, m_0 is the electron rest mass, ε_0 is the vacuum dielectric constant, M is the momentum matrix element (assumed to be of the form known for standard quantum wells), f_e and f_h are the Fermi-Dirac functions for the recombining carriers, and the density of states ρ_{QD} is assumed to be the following sum of the Gaussian distribution density functions:

$$\rho_{QD}(E) = \frac{1}{\sqrt{2\pi}} \sum_{i=1}^{K} \frac{1}{\Delta_i} \exp\left[-\frac{(E - E_i)^2}{2\Delta_i^2}\right]. \tag{16}$$

Values of the dispersions Δ_i and the energies E_i ($i = 1, 2, ..., K$)

$$E_i = E_G + i\hbar(\omega_e + \omega_h) \tag{17}$$

are taken from the plot of photoluminescence intensity versus wavelength. In the above equations, E_G is the energy gap and K is the number of photoluminescence peaks taken into consideration. During the fitting, Eq. (11) is providing an additional relation between ω_e and ω_h.

2.5. Interactions between individual physical phenomena. In the simulation, all four individual models and most of composing them physical processes are mutually interrelated by various important and often nonlinear interactions between individual physical phenomena therefore self-consistent algorithm of the calculations is necessary. Its flow chart is schematically shown in Fig. 1. More detailed description about our model was reported earlier [14].

3. The structure

The structure under consideration (Fig. 2) is the in-plane (edge-emitting) oxide-confined 1.3-μm quantum-dot (QD) (InGa)As/GaAs laser designed by Park et al. [2]. The laser is grown on the n-type GaAs substrate using the molecular-beam-epitaxy technology. Typically the structure consists lightly doped 2-μm p-type and n-type $Al_{0.85}Ga_{0.15}As$ cladding layers, which are covered with the high-Al-content 300-Å $Al_{0.98}Ga_{0.02}As$ layers and the 0.25-μm 12.5-period $GaAs/Al_{0.7}Ga_{0.3}As$ superlattice layers. All the above layers sandwich the laser waveguide and the gain region. The active region consists of the QD 10-monolayer $In_{0.5}Ga_{0.5}As$ (on the average) layer covered with the 15-monolayer $In_{0.09}Ga_{0.91}As$ layer. Achieved densities of quantum dots in this configuration are of the order of $2 \cdot 10^{10}$ cm^{-2}. This gain structure is sandwiched by the 150-Å GaAs layers and the 750-Å $Al_{0.05}Ga_{0.95}As$ waveguide layers. The whole structure is covered with the top 0.5-μm p^+-GaAs contact layer. Then the ridge structure is created by wet etching through the upper cladding layer. Next the high-Al-content layers are partly converted into the Al_xO_y layers with the aid of the wet oxidation technique to form an aperture W of 5 to 26 μm in width. Finally top stripe contacts (typically 40 μm) are fabricated. The resonator length L is typically equal to 870 μm.

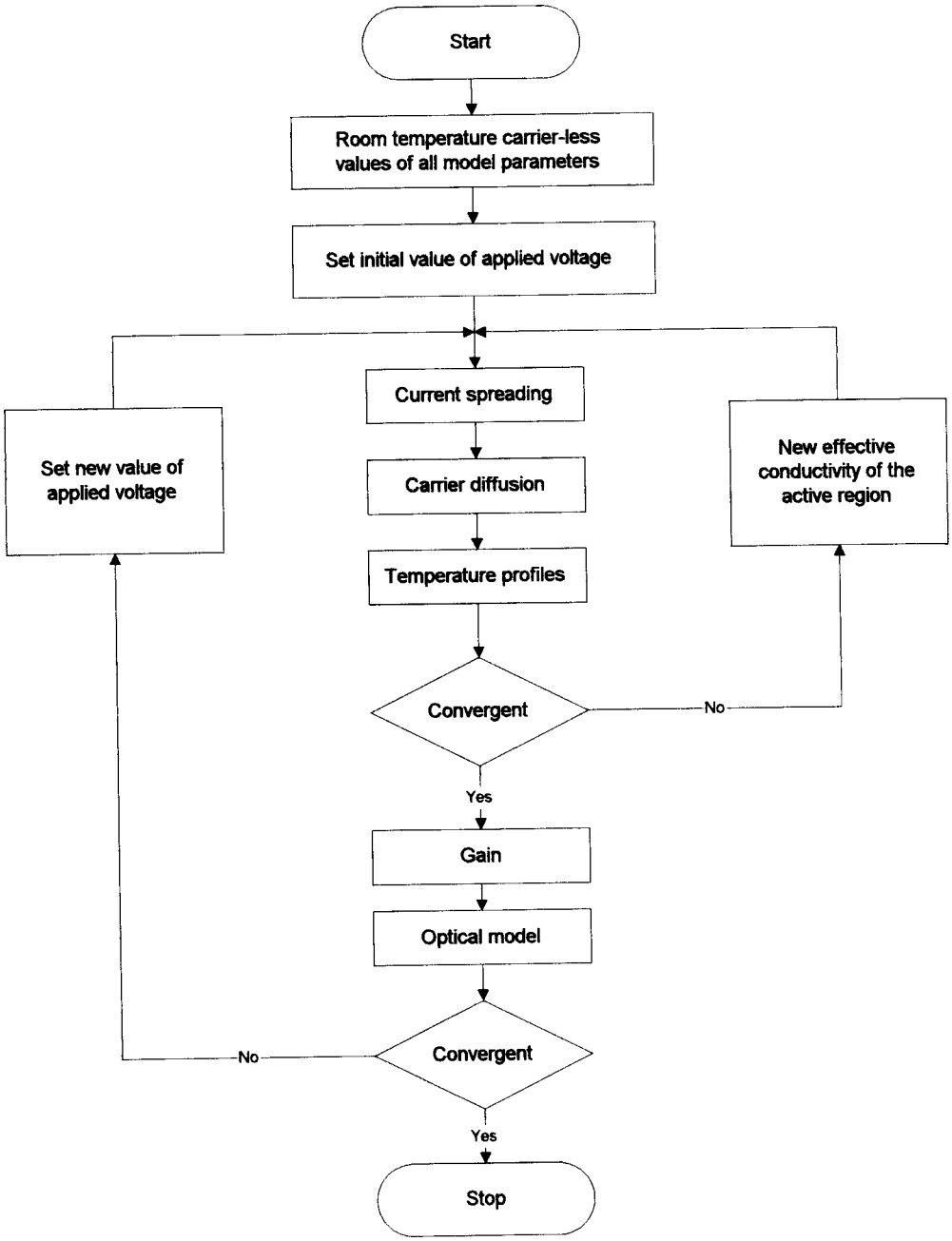

Fig. 1 Flow chart of the self-consistent approach used to simulate RT CW threshold characteristics of the 1.3-μm QD (InGa)As/GaAs laser

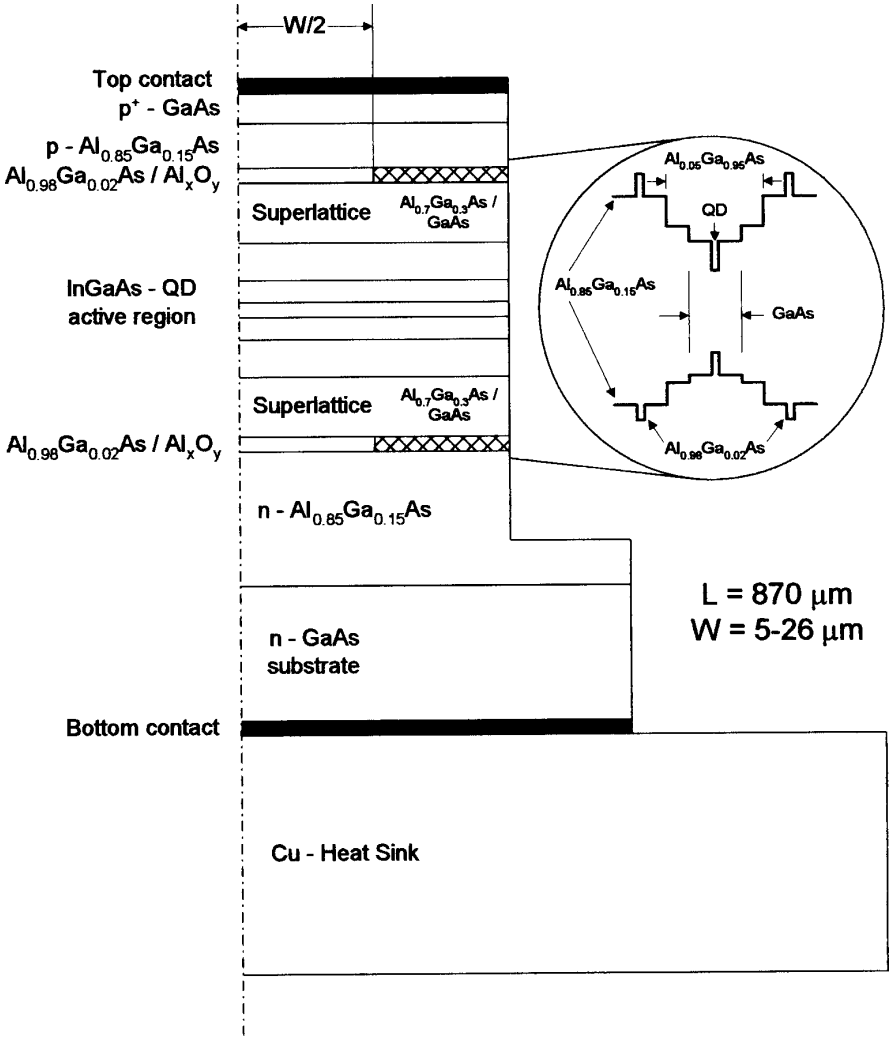

Fig. 2 An example structure of the oxide-confined 1.3-μm QD (InGa)As/GaAs laser [2]

4. Results

Let us use the model presented in Section 2 to describe physics of an operation of the in-plane oxide-confined 1.3-μm QD (InGa)As/GaAs laser shown in Section 3 to more deeply understand mutual interactions between individual physical processes crucial for a device operation and to anticipate laser performance characteristics. Besides, the model is intended to be used to optimise a laser structure for its room-temperature operation.

In Figure 3, aperture-width dependence of both the threshold current (left-hand axis) and the threshold current density (right-hand one) determined using the model presented in this paper are plotted as solid lines together with dashed lines presenting experimental results. As one can see, both pairs of curves are in a close agreement with each other, which allows us to believe that our self-consistent model is working properly and may be useful in simulation of performance characteristics of QD lasers under consideration.

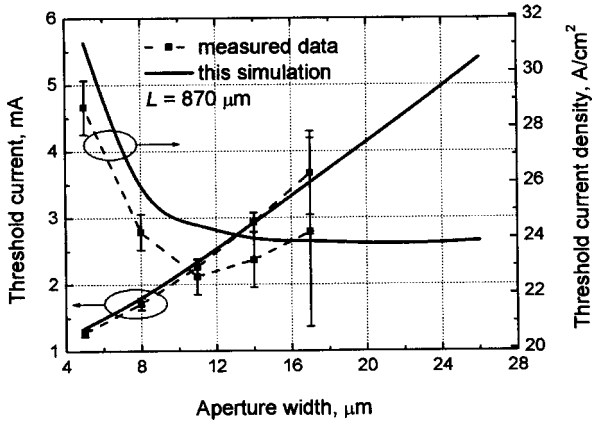

Fig. 3 The aperture-width dependence of the threshold current (left-hand axis) and the threshold current density (right-hand axis)

Figure 4 shows the optical gain versus the surface dot density dependence determined for various carrier concentrations. As one can see, each curve exhibits a distinct maximum, higher for higher carrier concentrations. Such

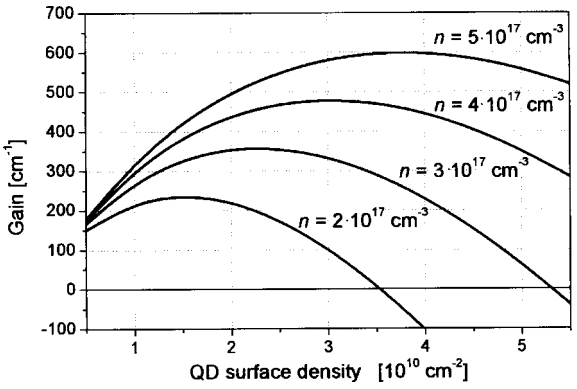

Fig. 4 The optical gain versus the QD surface density dependence for various carrier concentrations

a behaviour of the gain explains why there is a minimum in Fig 5, presenting the threshold-current-density dependence on the QD surface density. Hence it has been confirmed that there exists an optimal value of the QD density from the point of view of lasing-threshold reduction. Higher quantum-dot densities ensure, however, higher emitted power. This is caused by slow relaxation processes in quantum dots. So, as one can see, both requirements (i.e. low lasing threshold and high lasing output) are contradictory to each other. The above calculations were carried out under the assumption that the whole current is injected into the dots which seems to be well justified and is a better approximation for higher dot densities.

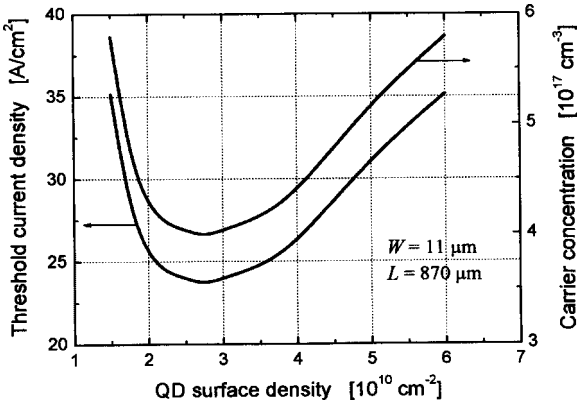

Fig. 5 The dependence of the threshold current density (left-hand axis) and the carrier concentration (right-hand axis) on the QD surface density

Figure 6 presents the Arrhenius-type temperature dependence of the lasing threshold. From the plot, the characteristic temperature $T_0 = 180$ K may be deduced. Its surprisingly high value may be associated with the assumption of negligible current leakage.

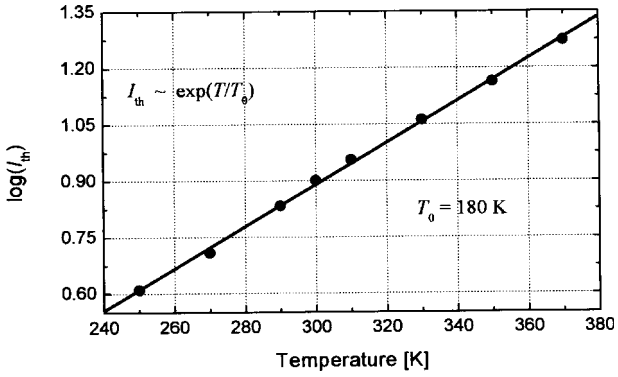

Fig. 6 Arrhenius-type temperature dependence of the lasing threshold enabling determination of the characteristic temperature $T_0 = 180$ K

5. Conclusions

First oxide-confined QD 1.3-μm arsenide laser has been already reported. Its structure, however, is still far from being optimal. Our self-consistent advanced model is intended to be used to simulate performance characteristics of the above laser and to optimise its structure. Currently, however, many numerical values of material and device parameters necessary in such modelling of GaAs-based quantum-dots devices are not available. Nevertheless, our slightly simplified simulation seems to remain quite exact with experimental characteristics known from literature and should be very useful in analysing the threshold operation characteristics of QD lasers and in optimisation of their structures for the low-threshold RT operation.

Acknowledgements. The work was supported by the Polish State Committee for Scientific Research (KBN), grants No 7-T11B-073-21 and No 4-T11B-014-25.

References

[1] D. Bimberg, M. Grundmann, N. N. Ledentsov, *Quantum Dot Heterostructures*, Chichester, Wiley, 1999.

[2] G. Park, O. B. Shchekin, D. L. Huffaker and D. G. Deppe, "Low-threshold oxide-confined 1.3-μm quantum-dot laser", *IEEE Photon. Techn. Lett.* 12, 230–232 (March 2000).

[3] K. S. Chiang, "Analysis of optical fibers by the effective-index method", *Applied Optics* 25, 348–354 (1986).

[4] D. I. Huffaker, G. Park, Z. Zou, O. B. Shchekin and D. G. Deppe, "Continuous-wave low-threshold performance of 1.3-μm InGaAs-GaAs quantum-dot lasers", *IEEE J. Sel. Topics Quantum Electron.* 6, 452–461 (2000).

[5] J. H. Shin, H. E. Shin and Y. H. Lee, "Effect of carrier diffusion in oxidized vertical-cavity surface-emitting lasers determined from lateral spontaneous emission", *Appl. Phys. Lett.* 70, 2652–2654 (1997).

[6] T. A. Strand, B. J. Thibeault and L. A. Coldren, "Reduced lateral carrier diffusion for improved miniature semiconductor lasers", *J. Appl. Phys.* 81, 3377–3381 (1997).

[7] G. Lengyel, P. Meissner, E. Patzak and K.-H. Zschauer, "An analytical solution of the lateral current spreading and diffusion problem in narrow oxide stripe (GaAl)As/GaAs DH lasers", *IEEE J. Quantum Electron.* QE– 18, 618–625 (1982).

[8] D. G. Deppe and Q. Deng, "Tunneling transport and diffusion in weakly coupled quantum dot ensembles", *Appl. Phys. Lett.* 73, 3536–3538 (1998).

[9] D. G. Deppe, D. L. Huffaker, S. Csutak, Z. Zou, G. Park and O. B. Shchekin, "Spontaneous emission and threshold characteristics of 1.3 μm InGaAs-GaAs quantum-dot GaAs-based lasers", *IEEE J. Quantum Electronics* 35, 1238–1246 (1999).

[10] M. Grundmann and D. Bimberg, "Theory of random population for quantum dots", *Phys. Rev. B* 55, 9740–9745 (1997).

[11] O. B. Shchekin and D. G. Deppe, "Low-threshold high-T_0 1.3-μm InAs quantum-dot lasers due to p-type modulation doping of the active region", *IEEE Photon. Techn. Lett.* 14, 1231–1234 (2002).

[12] M. Wasiak, M. Bugajski, R. P. Sarzała, P. Maćkowiak, T. Czyszanowski and W. Nakwaski, "Output power saturation in InAs/GaAs quantum dot lasers", *Physica status solidi (c)* 0, 1351–1354 (2003).

[13] M. Wasiak, M. Bugajski, E. Machowska-Podsiadło, T. Ochalski, J. Kątcki, R. P. Sarzała, P. Mackowiak, T. Czyszanowski, W. Nakwaski, J. X. Chen, U. Oesterle, A. Fiore and M. Ilegems, "Optical gain saturation effects in InAs/GaAs self-assembled quantum dots", *Optica Applicata* 32, 291–299 (2002).

[14] R. P. Sarzała, M. Wasiak, T. Czyszanowski, M. Bugajski and W. Nakwaski, "Threshold simulation of 1.3-μm oxide-confined in-plane quantum-dot (InGa)As/GaAs lasers", *Opt. Quantum Electron.* 35, 675–692 (2003).